Macromolecules

Cite This: Macromolecules 2018, 51, 9602−9612

Article

pubs.acs.org/Macromolecules

Ortho-Imide and Allyl Groups Effect on Highly Thermally Stable Polybenzoxazine/Double-Decker-Shaped Polyhedral Silsesquioxane Hybrids

Wei-Cheng Chen and Shiao-Wei Kuo*

Department of Materials and Optoelectronic Science, Center for Supramolecular Materials and Functional Polymers, National Sun Yat-Sen University, Kaohsiung 80424, Taiwan

Supporting Information

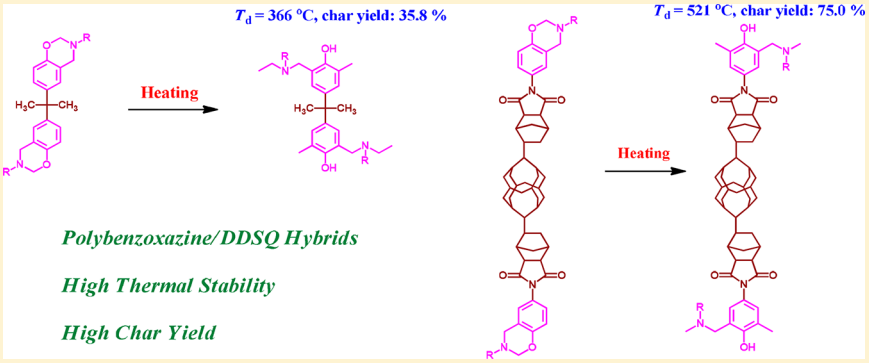

ABSTRACT: We synthesized double-decker silsesquioxane (DDSQ)-functionalized benzoxazine (BZ) monomers from a DDSQ prepared with nadic anhydride (ND) through hydrosilylation (to form DDSQ-ND) and then its reactions with *p*-aminophenol and *o*-aminophenol to form DDSQ-ND-*p*-OH and DDSQ-ND-*o*-OH, respectively. Four different DDSQ-functionalized BZ monomers were prepared through reacting DDSQ-ND-*p*-OH and DDSQ-ND-*o*-OH with CH_2O and either aniline or allylamine: *p*BDDSQ-AN, *p*BDDSQ-AL, *o*BDDSQ-AN, and *o*BDDSQ-AL. All of these polybenzoxazine (PBZ)/DDSQ hybrids exhibited high thermal stability and high char yields after thermal curing, based on thermogravimetric analysis (TGA), because the DDSQ inorganic nanoparticles were dispersed homogeneously in the PBZ matrices, as evidenced using electron microscopy. For example, the thermal decomposition temperature (T_d) and char yield of *p*BDDSQ-AN after thermal curing at 270 °C were 521 °C and 75 wt %, respectively. More interestingly, the char yield of the *ortho*-substituted *o*BDDSQ-AN increased from 72.7 wt % prior to thermal treatment to 76.0 wt % after thermal treatment at 450 °C, indicating that the polybenzoxazole may have formed after such thermal treatment to increase the char yield, which was higher than that of the *para*-substituted *p*BDDSQ-AN.

INTRODUCTION

Benzoxazine (BZ) chemistry has received much attention during recent years because of the flexible molecular design, high dimensional stability, stable dielectric constants, good flame retardancy, and low surface free energy after thermal curing—properties that are not observed in traditional epoxy or phenolic resins.[1−11] BZ derivatives are six-membered heterocyclic monomers featuring nitrogen and oxygen atoms in the oxazine ring; they are synthesized through facile Mannich condensations from phenolic derivatives, primary aromatic or aliphatic amines, and CH_2O, in various solvents. A BZ monomer can undergo self-cross-linking through thermal ring-opening polymerization to form a polybenzoxazine (PBZ) having a three-dimensional (3D) cross-linked structure, without releasing any byproducts.[12−17]

Unfortunately, PBZs have limited applications at relatively high temperatures because their C−N−C bonds readily break at temperatures higher than 260 °C.[18] Several strategies have been tested to enhance the thermal stability of PBZs. For example, introducing allyl or alkynyl units into the BZ monomers can enhance the cross-linking density of the 3D network structure;[19−25] with this approach, the resulting PBZs can exhibit higher glass transition temperatures, superior mechanical properties, and greater solvent resistance. Alternatively, blending with other polymers can form miscible blend systems,[26−28] or blending with inorganic nanomaterials can vary the thermal properties through decreasing chain mobility. The most widely reported inorganic nanomaterials used to form PBZ hybrids have been carbon-based (e.g., carbon black,[29] carbon nanotubes,[30−35] and graphene[36−38]) and silicon-based (e.g., polydimethylsiloxane (PDMS),[39,40] nanoclay silicates,[41−43] and polyhedral oligomeric silsesquioxane

Received: October 14, 2018
Revised: November 14, 2018
Published: November 21, 2018

DOI: 10.1021/acs.macromol.8b02207
Macromolecules 2018, 51, 9602−9612

Scheme 1. Synthesis of (g, h) DDSQ-Functionalized DDSQ BZ Monomers from (a) Phenyltrimethoxylsilane, (b) DD-Na, (c) DDSQ, (d) DDSQ-ND, (e) DDSQ-ND-*p*-OH, and (f) DDSQ-ND-*o*-OH

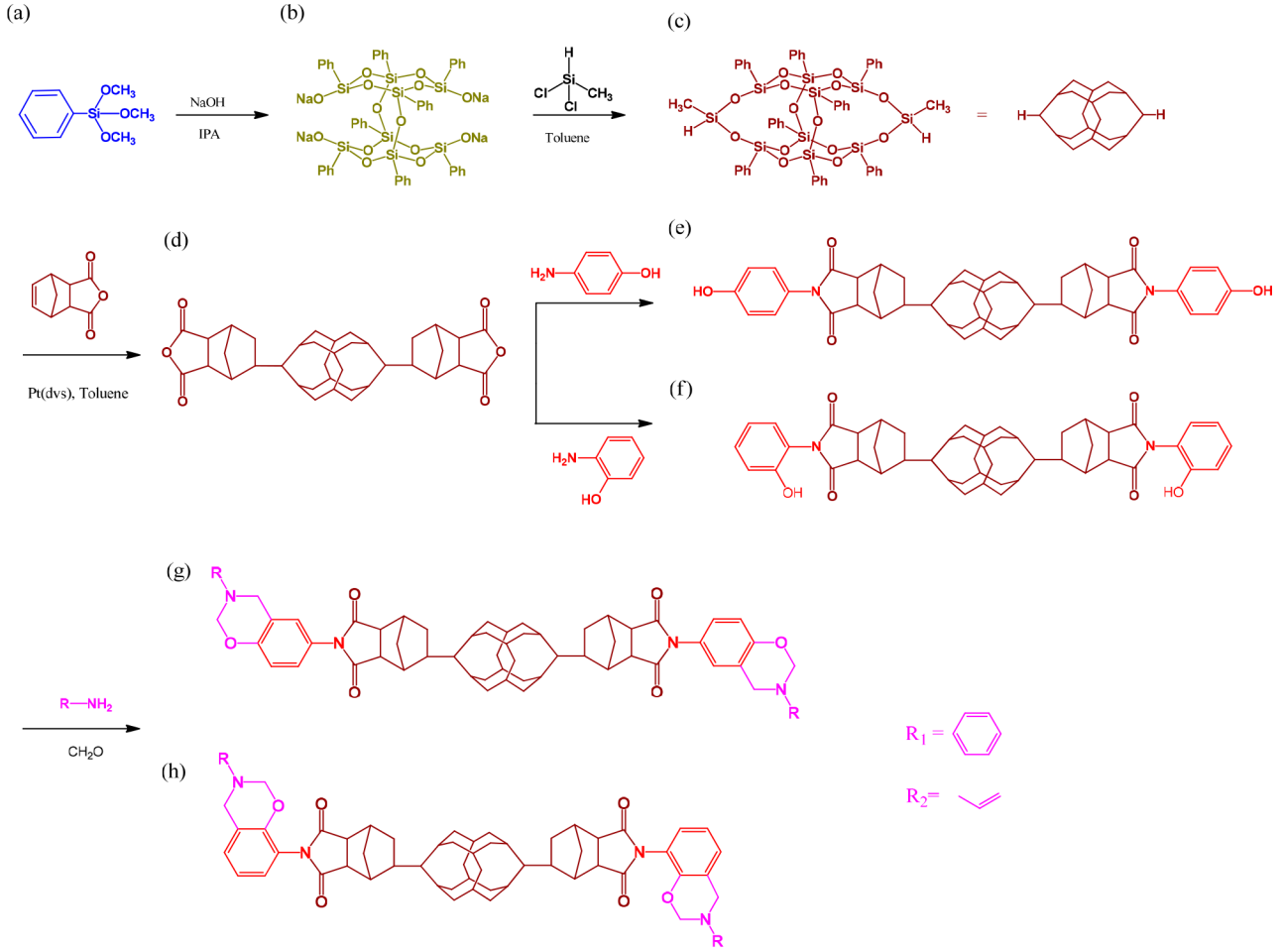

(POSS)[43−57]) materials. POSS derivatives are precisely structured inorganic building blocks of nanometer dimensions; they have been introduced into many different polymer matrices to form organic/inorganic nanocomposites. For PBZ/POSS hybrids, most previous examinations have used mono- and octafunctionalized POSS BZ monomers to form the organic/inorganic nanocomposites.[43−54] For example, we prepared mono- and octafunctionalized POSS macromers with BZ units and then blended them with mono- or difunctionalized BZ monomers to form organic/inorganic nanocomposites.[43−50] In those studies, all of the POSS macromers were derivatized with mono- or multifunctionalized BZ monomers and formed only low-molecular-weight PBZ/POSS hybrids. Several approaches have been tested to result in difunctionalized POSS macromers forming high-molecular-weight main-chain-type PBZs.[55−57] For example, Zheng et al. used a dianilino double-decker silsesquioxane (DDSQ) with bisphenol A and CH_2O to form a main chain type of PBZ with DDSQ.[56] We have also prepared a transparent and flexible DDSQ-BZ-PDMS copolymer through Mannich condensation of allyl amide, CH_2O, and a bifunctionalized phenolic DDSQ compound (DDSQ-BP) to obtain a bis-allyl BZ DDSQ (DDSQ-BZ) that we then reacted with PDMS through hydrosilylation.[55]

Recently, Ishida et al. proposed another way to obtain highly thermally and mechanically stable PBZs: through thermal conversion from *ortho*-functionalized BZs, leading to highly thermal stable polybenzoxazoles (PBOs).[58−62] These PBOs could have formed from *ortho*-imide-, *ortho*-amide-, and *ortho*-amide/imide-functionalized BZs through thermal conversions at relatively high temperatures (>400 °C).[58−62] In general, the thermal stability of *ortho*-functionalized PBZs is better than that of PBZs formed from *para*-functionalized BZ monomers. The introduction of allyl units or the use of *ortho*-functionalized BZs can improve the thermal stability, as mentioned earlier; although these individual approaches have been investigated widely,[19−23,58−62] the effects of incorporating inorganic DDSQ nanoparticles into allyl- and *ortho*-functionalized BZ monomers, together, remain poorly understood.

In this study, we synthesized four different DDSQ-functionalized BZ monomers as displayed in Scheme 1. First we synthesized two different bifunctionalized phenolic units, with *para*- and *ortho*-stereochemistry, based on DDSQ from phenyltrimethoxylsilane and DD-Na (Scheme 1b), with subsequent hydrosilylation with nadic anhydride (ND) giving DDSQ-ND (Scheme 1d). DDSQ-ND-*p*-OH (Scheme 1e) and DDSQ-ND-*o*-OH (Scheme 1f) were obtained after reacting *p*-aminophenol and *o*-aminophenol with DDSQ-ND, respectively. We then prepared four different DDSQ-functionalized BZ monomers from DDSQ-ND-*p*-OH and DDSQ-ND-*o*-OH reacting with CH_2O and aniline or allylamine, as displayed in Schemes 1g and 1h. Thereafter, we investigated the influences of the allyl units, the *ortho*-imide functionality, and the DDSQ

DOI: 10.1021/acs.macromol.8b02207
Macromolecules 2018, 51, 9602−9612

inorganic nanoparticles on the thermal stability and curing behavior of these four BZ monomers.

EXPERIMENTAL SECTION

Materials. Methyldichlorosilane, phenyltrimethoxylsilane, sodium hydroxide (NaOH), platinum divinyltetramethyldisiloxane complex [Pt(dvs)], tetrahydrofuran (THF), magnesium sulfate ($MgSO_4$), 2-propanol, and charcoal were purchased from Alfa-Aesar. ND, methanol (MeOH), ethanol (EtOH), sodium bicarbonate ($NaHCO_3$), *n*-hexane, 1,4-dioxane, ethyl acetate, *p*-aminophenol, *o*-aminophenol, aniline, allylamine, and paraformaldehyde were purchased from Sigma-Aldrich.

Double-Decker Silsesquioxane-Na (DD-Na).[55] A mixture of phenyltrimethoxylsilane (210 g, Scheme 1a), NaOH (28 g), deionized H_2O (20 mL), and 2-propanol (600 mL) was heated for 24 h under reflux in a flask equipped with a reflux condenser. The mixture was stirred for further 8 h at room temperature until the reaction was complete. The solvent was evaporated through vacuum distillation, and the residue was dried in a vacuum oven to give a white powder (138 g, 90%, Scheme 1b).

Double-Decker Silsesquioxane.[55] A mixture of DD-Na (5.80 g, 5.00 mmol), triethylamine (2.00 g, 20.0 mmol), and THF (100 mL) was stirred thoroughly in an ice bath, and then methyldichlorosilane (2.25 g, 20.0 mmol) was added as an end-capping agent. The mixture was stirred at room temperature for 6 h, the filtrate and an equal volume of a saturated aqueous solution of $NaHCO_3$ were poured into a separating funnel, and the organic phase was separated (the upper layer). After magnesium sulfate ($MgSO_4$) was added in organic phase and stirred for 30 min, the mixture was filtered to give a clear filtrate, which was concentrated under reduced pressure to remove solvent and placed in a vacuum oven at 40 °C. After drying, a white solid was obtained (2.2 g, 38%, Scheme 1c).

Bis-(Nadic Anhydride) Double-Decker Silsesquioxane (DDSQ-ND). DDSQ (5.00 g, 4.34 mmol), ND (1.57 g, 9.55 mmol), and toluene (200 mL) were placed in a flask equipped with a reflux condenser. Pt(dvs) (5 drops) was added, and then the mixture was heated at 75 °C for 48 h under a N_2 atmosphere. The resulting mixture was filtered through charcoal, and the filtrate was concentrated through vacuum distillation. The residue was washed three times with EtOH and then dried in a vacuum oven at 105 °C to give a white solid (6.4 g, 92%, Scheme 1d).

Bis-Phenolic Double-Decker Silsesquioxanes (DDSQ-ND-OH). A solution of *p*-aminophenol (2.80 g, 27.2 mmol) in DMF (20 mL) was added gradually to a solution of DDSQ-ND (6.00 g, 13.0 mmol) in DMF (60 mL). The mixture was stirred in an ice bath for 8 h, and then a Dean−Stark apparatus was used to perform the imidization reaction. A solid powder was obtained after vacuum distillation; it was recrystallized from isopropanol. DDSQ-ND-*p*-OH was formed as a dark brown powder (6.06 g, 90%, Scheme 1e); DDSQ-ND-*o*-OH was formed as a red powder in the corresponding reaction with *o*-aminophenol (5.79 g, 86%, Scheme 1f).

Bis-Aniline BZ Double-Decker Silsesquioxane (BDDSQ-AN). DDSQ-ND-OH (2.39 g, 1.44 mmol), CH_2O (0.174 g, 5.75 mmol), and 1,4-dioxane (50 mL) were placed in a flask equipped with a reflux condenser. After three cycles of purging with N_2 gas, the aniline derivative (0.267 g, 2.88 mmol) was added. The mixture was heated at 115 °C for 48 h. After cooling, the mixtures were subjected to gravity filtration. The solvent was evaporated using a rotary evaporator, and then the residue was dried in a vacuum oven to give a powder. *p*BDDSQ-AN was obtained as a brown powder when using DDSQ-ND-*p*-OH (1.91 g, 70%, Scheme 1g-R_1); *o*BDDSQ-ND-AN was obtained as an orange powder when using DDSQ-ND-*o*-OH (1.75 g, 64%, Scheme 1h-R_1).

Bis-Allyl BZ Double-Decker Silsesquioxane (BDDSQ-AL). DDSQ-ND-OH (2.39 g, 1.44 mmol), CH_2O (0.348 g, 11.5 mmol), and *p*-xylene (50 mL) were placed in a flask equipped with a reflux condenser. After three cycles of purging with N_2, allylamine (0.328 g, 5.74 mmol) was added. The mixture was heated at 90 °C for 48 h. After cooling, the mixture was subjected to gravity filtration. The solvent was evaporated using a rotary evaporator, and the residue was dried in a vacuum oven to give a powder. The reaction of DDSQ-ND-*p*-OH provided *p*BDDSQ-AL as a yellow powder (1.97 g, 75%, Scheme 1g-R_2); the reaction of DDSQ-ND-*o*-OH provided *o*BDDSQ-AL as an orange powder (1.86 g, 71%, Scheme 1h-R_2).

Thermal Curing of BDDSQ-AN and BDDSQ-AL Monomers. Desired amounts of the various BZ monomers were placed in an aluminum dish and heated in steps at 150, 180, 210, 240, and 270 °C, each for 2 h, in a vacuum oven. Each cured sample had a red color that became darker as the thermal curing temperature increased.

Characterization. NMR spectra were recorded by using an INOVA 500 instrument, with DMSO-d_6 and $CDCl_3$ as solvents. Fourier transform infrared (FTIR) spectra of the DDSQ derivatives were recorded using a Bruker Tensor 27 FTIR spectrophotometer. The conventional KBr disk method was used, with 32 scans collected at a spectral resolution of 4 cm^{-1}. The prepared samples were sufficiently thin to obey the Beer−Lambert law. The molecular weights of the DDSQ derivatives were determined using a Bruker Daltonics Autoflex MALDI-TOF mass spectrometer. The dynamic curing behavior of the DDSQ-functionalized BZ monomers under N_2 was recorded using a TA Q-20 DSC instrument; the dynamic curing thermograms were measured from 20 to 360 °C at a heating rate of 20 °C/min. The thermal stabilities—characterized by thermal decomposition temperatures (10 wt % loss) and char yields—of the DDSQ-functionalized BZ monomers were recorded under N_2 using a TA Q-50 TGA apparatus; those samples were examined from 50 to 800 °C at a heating rate of 20 °C/min. To investigate the phase behavior of the PBZ/DDSQ hybrids, each sample surface was coated with a thin layer of Au (ca. 100 Å). The thermally cured samples were investigated using an FEI Quanta 200 environmental scanning electron microscope (SEM) operated at 5 kV. Transmission electron microscopy (TEM) was performed using a JEOL-2100 electron microscope operated at 200 kV. Ultrathin sections (thickness: 700 Å) of the PBZ/DDSQ hybrids were prepared at room temperature using a Leica Ultracut S microtome equipped with a diamond knife. The ultrathin samples were placed onto a Cu grid, which was coated with a carbon supporting film, without further staining.

RESULTS AND DISCUSSION

Synthesis of DDSQ-Functionalized BZ Monomers. Scheme 1 displays the synthesis of the DDSQ-functionalized BZ monomers. The chemical structure at each step was identified using ^1H NMR and FTIR spectroscopy and MALDI-TOF mass spectrometry. For example, Figure 1 displays the FTIR spectrum of each compound during the synthesis of *p*BDDSQ-AN and *p*BDDSQ-AL, with *para*-imide BZ monomers. A strong absorption at 1097 cm^{-1} (corresponding to Si−O−Si units) and an absorption at 1261 cm^{-1} (corresponding to Si−CH_3 units) were general features in the spectrum of each DDSQ derivative.[55] In addition, a Si−H stretching signal appeared at 2172 cm^{-1} in the spectrum of pure DDSQ, as displayed in Figure 1a; this signal disappeared after hydrosilylation with ND, but signals for two new anhydride C=O units appeared at 1860 and 1782 cm^{-1} for DDSQ-ND, as displayed in Figure 1b, confirming the success of this transformation. The spectrum of DDSQ-ND-*p*-OH (Figure 1c) exhibits a broad absorption at 3395 cm^{-1} for OH stretching, two sharp absorptions at 1700 and 1771 cm^{-1} for imide C=O stretching, and an absorption at 1390 cm^{-1} for C−N stretching, and lower-wavenumber shifts of the signals for C=O stretching and OH stretching, consistent with the formation of DDSQ-ND-*p*-OH. The spectra of the BZ monomers *p*BDDSQ-AN (Figure 1d) and *p*BDDSQ-AL (Figure 1e) both feature signals for imide C=O stretching—both red-shifted to 1709 and 1772 cm^{-1}—and signals for the BZ ring structures at 1499, 1235, and 939 cm^{-1} for

DOI: 10.1021/acs.macromol.8b02207
Macromolecules 2018, 51, 9602−9612

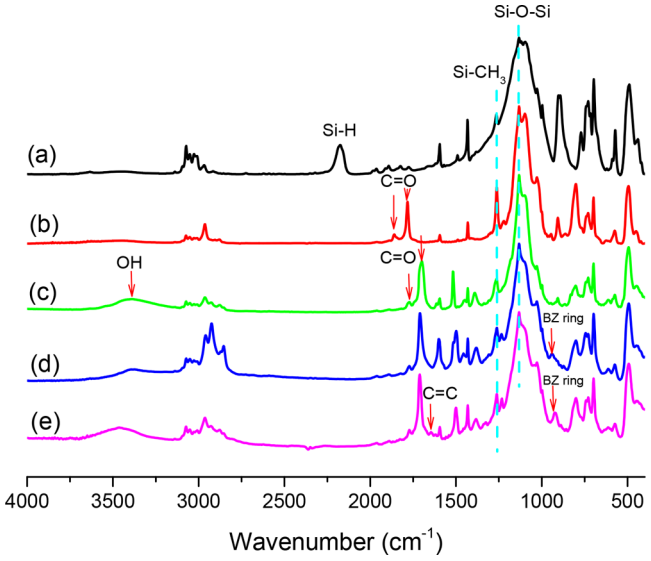

Figure 1. FTIR spectra of (a) DDSQ, (b) DDSQ-ND, (c) DDSQ-ND-*p*-OH, (d) *p*BDDSQ-AN, and (e) *p*BDDSQ-AL.

*p*BDDSQ-AN and 1500, 1232, and 923 cm^{-1} for *p*BDDSQ-AL; an additional signal for C═C stretching appeared at 1644 cm^{-1} in the spectrum of *p*BDDSQ-AL. The FTIR spectra of *o*BDDSQ-AN and *o*BDDSQ-AL, with *ortho*-imide BZ monomers, had similar features (Figure S1).

Figure 2 displays the corresponding ^{1}H NMR spectra of *p*BDDSQ-AN and *p*BDDSQ-AL, with *para*-imide BZ monomers. The signals for the Si−H and $SiCH_3$ units were located at 4.98 ppm (peak a) and 0.36 ppm, respectively, while the signals for the aromatic protons appeared between 7.14 and 7.50 ppm (Figure 2a). The Si−H signal disappeared after hydrosilylation with ND to provide DDSQ-ND (Figure 2b). Signals for two isomers were observed after hydrosilylation of the vinyl units of ND, representing α- and β-configurations. Various signals for the aliphatic protons appeared between 0.83 and 3.25 ppm: for example, at 3.25−3.20 (i), 2.89 (j), 1.80−1.57 (f−h,), 1.28 (e), and 0.83 (d) ppm; we did not observe

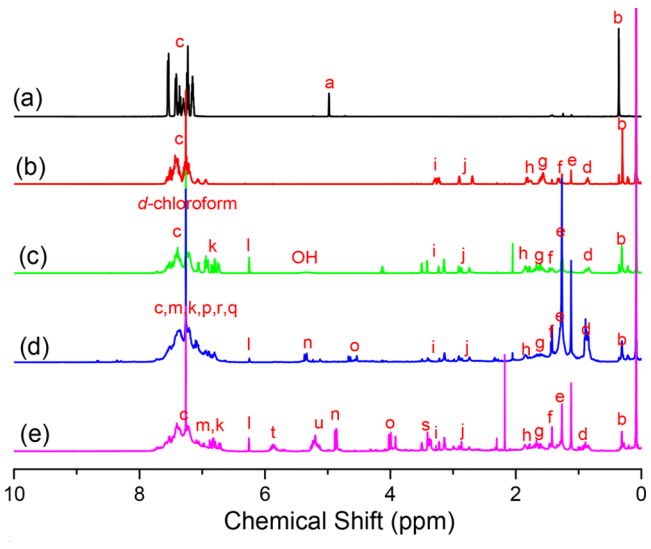

Figure 2. ^{1}H NMR spectra of (a) DDSQ, (b) DDSQ-ND, (c) DDSQ-ND-*p*-OH, (d) *p*BDDSQ-AN, and (e) *p*BDDSQ-AL.

any signals for any residual vinyl units in DDSQ-ND.[63,64] The spectrum of DDSQ-ND-*p*-OH (Figure 2c) exhibits a broad signal at 5.33 ppm for the OH groups and signals for the aromatic protons of *p*-aminophenol at 6.80 (k) and 6.24 (l) ppm, consistent with the formation of DDSQ-ND-*p*-OH. The signal for the phenolic OH groups disappeared, and signals for the BZ ring (methylene bridge protons) appeared at 4.65 ppm (o, $ArCH_2N$) and 5.30 ppm (n, OCH_2N), as displayed in Figure 2d, for *p*BDDSQ-AN; in contrast, these two signals were observed at 3.98 ppm (o) and 4.86 ppm (n) for *p*BDDSQ-AL (Figure 2e). The different chemical shifts of the signals in these BZ rings resulted from the different functional groups when reacting aniline and allylamine as the primary amines. In addition, in the spectrum of *p*BDDSQ-AL we observed signals for the vinyl unit at 5.16 and 5.87 ppm, in a 2:1 ratio, and for the proton between the nitrogen atom and the vinyl unit appeared at 3.30 ppm (s). The ^{1}H NMR spectra of *o*BDDSQ-AN and *o*BDDSQ-AL, with *ortho*-imide BZ monomers, displayed similar features (Figure S2). Notably, however, the spectrum of DDSQ-ND-*o*-OH (Figure S2c) exhibits a broad signal at 4.90 ppm for the OH unit, with the signals for the aromatic protons of the 2-aminophenol unit appearing at 6.72 (k) and 6.26 (l) ppm. The different chemical shifts of the signals for the phenolic OH units of DDSQ-ND-*o*-OH with DDSQ-ND-*p*-OH arose because of intramolecular hydrogen bonding of the phenolic OH unit with the imide C═O unit.[58−62] In addition, the signals of the BZ ring (methylene bridge protons) appeared at 4.63 ppm (o, $ArCH_2N$) and 5.33 ppm (n, OCH_2N) for *o*BDDSQ-AN (Figure S2d), whereas the two signals appeared at 3.99 (o) and 4.88 (n) ppm for *o*BDDSQ-AL (Figure S2e). For *o*BDDSQ-AL, the signals for the vinyl protons were observed at 5.19 and 5.84 ppm, in a 2:1 ratio, and the signal for the protons between the nitrogen atom and the vinyl unit appeared at 3.37 ppm (s). Scheme S1 displays all of the other peaks assignment for the four DDSQ-functionalized BZ monomers.

Figure 3 presents the MALDI-TOF mass spectra of the corresponding DDSQ compounds: the signal for $[DDSQ + Na]^+$ appeared as a monodisperse mass distribution at 1176 g/mol, while those for $[DDSQ\text{-}ND + Na]^+$ and $[DDSQ\text{-}ND\text{-}p\text{-}OH + Na]^+$ were located at 1504 and 1685 g/mol, respectively. We also observed signals at 1921 g/mol for [*p*DDSQ-AN +

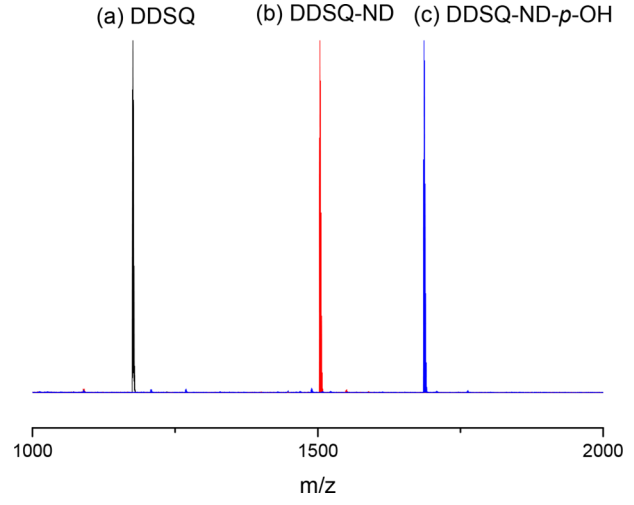

Figure 3. MALDI-TOF mass spectra of (a) DDSQ, (b) DDSQ-ND, and (c) DDSQ-ND-*p*-OH.

DOI: 10.1021/acs.macromol.8b02207
Macromolecules 2018, 51, 9602−9612

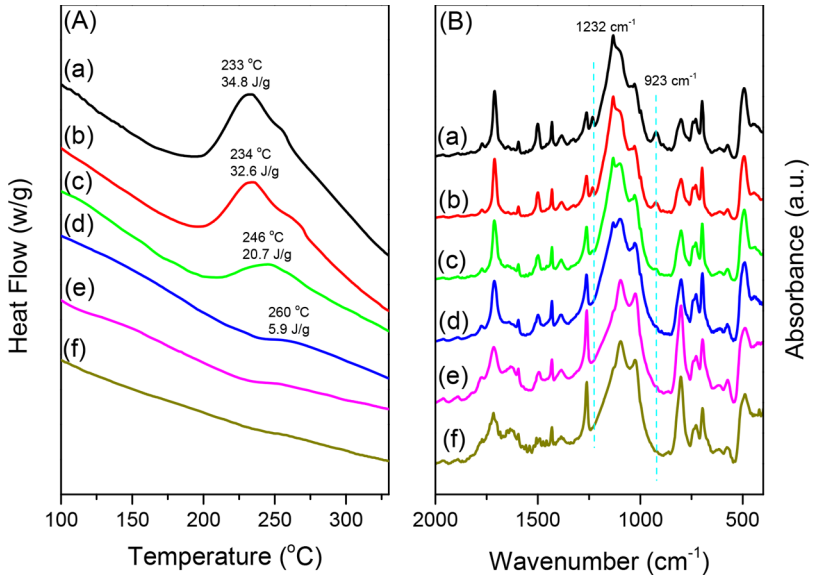

Figure 4. (A) DSC traces and (B) FTIR spectra of uncured *p*BDDSQ-AL, recorded after each curing stage: (a) uncured, (b) 150 °C, (c) 180 °C, (d) 210 °C, (e) 240 °C, and (f) 270 °C.

Scheme 2. (a–d) Thermal Ring-Opening Polymerization of (b) from (a) *p*BDDSQ-R and (d) from (c) *o*BDDSQ-R; (e) Intramolecular Hydrogen Bonding of Phenolic OH and Imide C═O Groups; (f) Thermal Conversion Behavior of the *o*BDDSQ-R Monomer

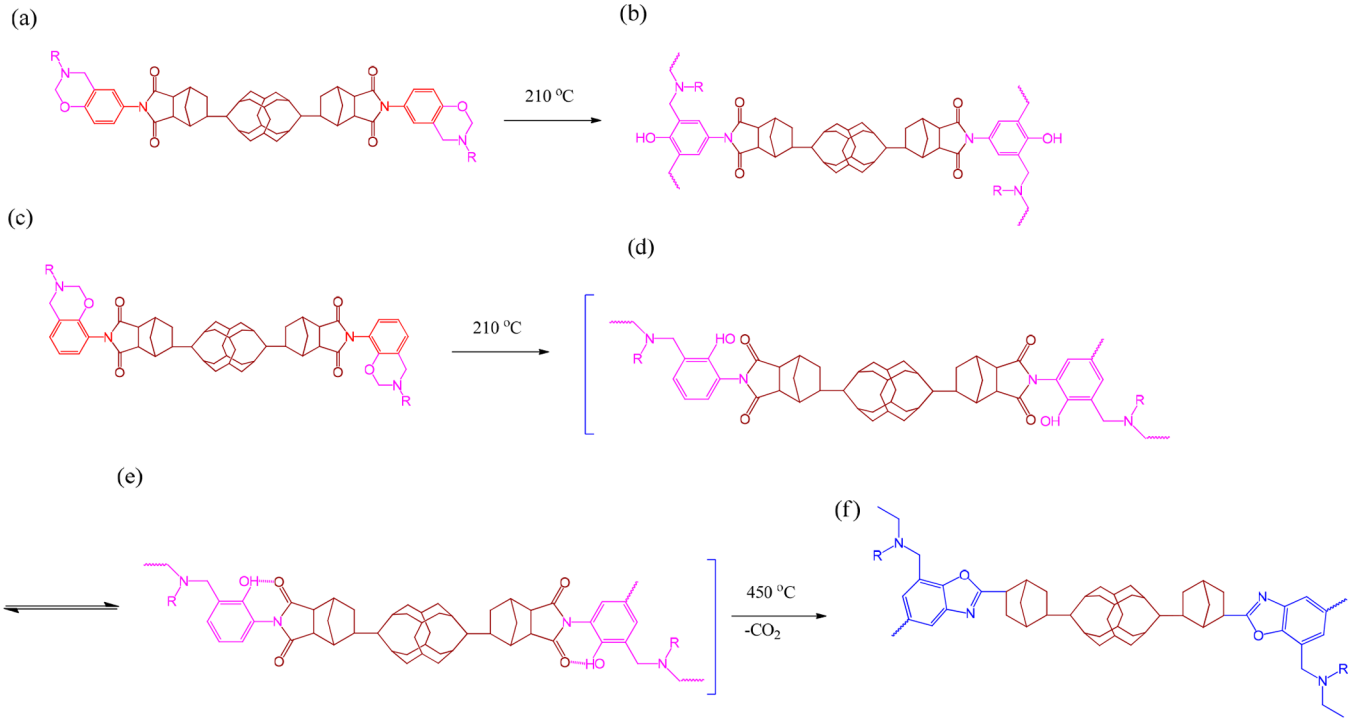

Na]$^+$ and 1848 g/mol for [*p*DDSQ-AL + Na]$^+$ (Figure S3). Several peaks appeared below these signal for the molecular ions, presumably because of decomposition of the BZ monomers during the mass spectral analyses.[16,65] The experimental and calculated molecular weights were in good agreement, consistent with the well-defined structures of these DDSQ derivatives. Considering all of the FTIR, NMR, and mass spectral data, we had successfully synthesized these four DDSQ-functionalized BZ monomers.

Thermal Curing Behavior of DDSQ-Functionalized BZ Monomers. We use DSC to investigate the thermal curing behavior of the DDSQ-functionalized BZ monomers. Figure 4A displays the DSC thermograms of the *p*BDDSQ-AL BZ monomer after each thermal curing process; a thermal curing exothermic peak appeared at 233 °C, with a reaction heat of 34.8 J/g for the uncured *p*BDDSQ-AL monomer (Figure 4A-a). The reaction heat of *p*BDDSQ-AL decreased upon increasing the curing temperature. In addition, the exothermic peak disappeared completely when the curing temperature was >240 °C (Figure 4A-e), implying that the thermal curing temperature of *p*BDDSQ-AL was >240 °C. This phenomenon of thermal curing of *p*BDDSQ-AL was confirmed through

DOI: 10.1021/acs.macromol.8b02207
Macromolecules 2018, 51, 9602–9612

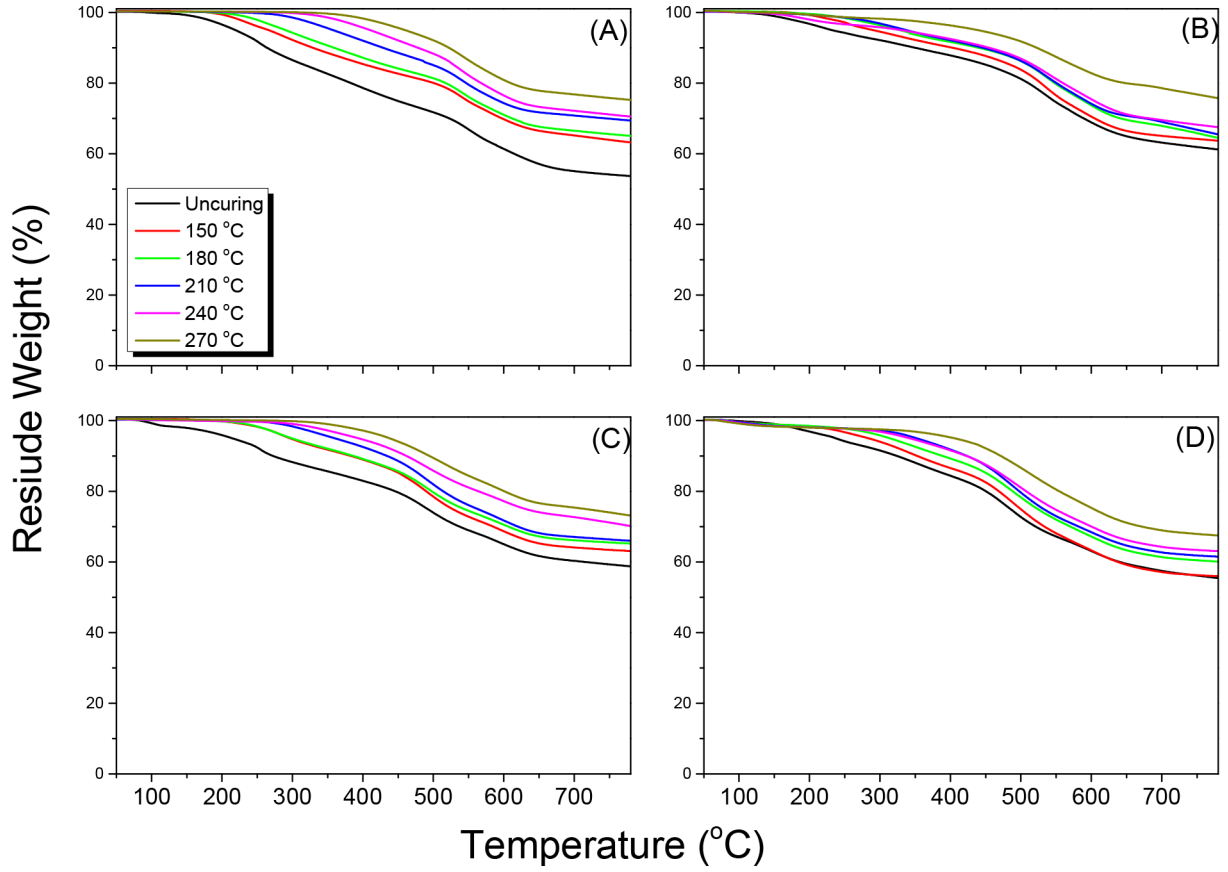

Figure 5. TGA traces of four DDSQ-functionalized BZ monomers, recorded after each curing stage: (A) *p*BDDSQ-AN, (B) *p*BDDSQ-AL, (C) *o*BDDSQ-AN, and (D) *o*BDDSQ-AL.

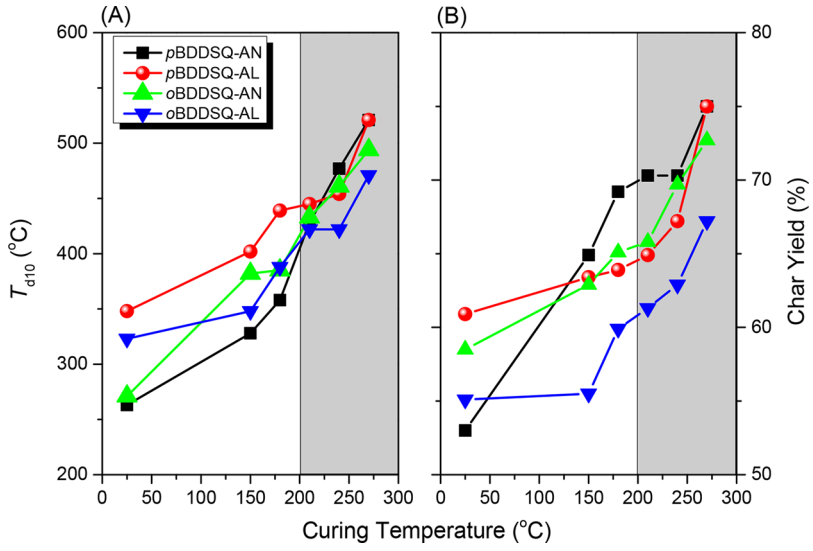

Figure 6. (A) Thermal decomposition temperatures and (B) char yields of the four DDSQ-functionalized BZ monomers, recorded after each curing stage.

FTIR spectroscopic analysis (Figure 4B); the major absorption peaks of the uncured *p*BDDSQ-AL were located at 923 cm^{-1} (oxazine ring), 1232 cm^{-1} (C−O−C), and 1644 cm^{-1} (C═C stretching). The intensities of these characteristic absorption peaks gradually decreased upon increasing the thermal curing temperature and disappeared completely when the thermal curing temperature was 240 °C (Figure 4B-e). We observed similar results for the thermal curing of the *o*BDDSQ-AL monomer (Figure S4). A thermal curing exothermic peak appeared at 222 °C, with a reaction heat of 24.8 J/g, for the uncured *o*BDDSQ-AL monomer (Figure S4A-a); the intensity of the peak for the reaction heat of *o*BDDSQ-AL also decreased upon increasing the thermal curing temperature and disappeared completely when the curing temperature was >240 °C (Figure S4A-e). The lower curing temperature of the *o*BDDSQ-AL monomer (222 °C), compared with that of the

DOI: 10.1021/acs.macromol.8b02207
Macromolecules 2018, 51, 9602−9612

*p*BDDSQ-AL monomer (233 °C), indicated that the *ortho* substitution of aminophenol, featuring intramolecular hydrogen bonding of the phenolic OH and imide C═O groups, after thermal curing, could improve the ring-opening polymerization of the BZ monomer. The intensity of the main absorption peak of the uncured *o*BDDSQ-AL, located at 916 cm^{-1} (oxazine ring), also decreased gradually upon increasing the thermal curing temperature and disappeared completely when the thermal curing temperature was 240 °C (Figure S4B-e). The FTIR spectra of the *p*BDDSQ-AL and *o*BDDSQ-AL BZ monomers both featured a broad peak between 1650 and 1800 cm^{-1}, as displayed in Figure 4B-f and Figure S4B-f, respectively, due to intermolecular hydrogen bonding of the phenolic OH and C═O groups after thermal curing (Scheme 2e). Therefore, the FTIR spectra and the DSC thermal analyses were consistent in implying that the BZ rings would be opened thermally to form highly cross-linked PBZ/DDSQ hybrids without the need for a catalyst.

Thermal Properties of DDSQ-Functionalized BZ Monomers. We used TGA to study the thermal stabilities of these DDSQ-functionalized BZ monomers (Figure 5). The TGA thermograms were recorded at temperature ranging from 50 to 800 °C, at a heating rate of 20 °C/min, under a N_2 atmosphere. We used the 10% weight loss temperature (T_{d10}) as the standard; this value and the corresponding char yield (summarized in Figure 6) both increased upon increasing the thermal curing temperature for our four different DDSQ-functionalized BZ monomers. The uncured *p*BDDSQ-AN monomer provided a value of T_{d10} of 263 °C and a char yield of 53% (Scheme 2a); after thermal curing, these values were 521 °C and 75%, respectively (Scheme 2b). For the *p*BDDSQ-AL monomer, the value of T_{d10} was 348 °C and the char yield was 60.9%; they reached 521 °C and 75%, respectively, after thermal curing. These two PBZs, based on *p*BDDSQ-AN and *p*BDDSQ-AL, both exhibited thermal stability (T_{d10} = 521 °C) higher than those of any other reported PBZs, presumably because the DDSQ cage structures enhanced the thermal resistance after thermal curing. More interestingly, these two values were very similar for the *p*BDDSQ-AN and *p*BDDSQ-AL monomers, indicating that the presence of the aniline or allylamine functionality did not affect the thermal stability after thermal curing. Nevertheless, these two values were different at the different curing temperature stages, with the values of T_{d10} for *p*BDDSQ-AL being higher than those for *p*BDDSQ-AN, probably because of the extra cross-linking density arising from the allyl units of *p*BDDSQ-AL after thermal curing. In contrast, the char yields of *p*BDDSQ-AN were higher than those of *p*BDDSQ-AL at the different curing temperature stages, implying that the aliphatic methylene (CH_2) unit in allyl group was relatively easy to break during thermal heating at relatively lower temperatures.[19] This result is similar to that of *o*BDDSQ-AN providing a higher char yield than *o*BDDSQ-AL. A lower char yield from the allylamine-based BZ monomer was also apparent when we compared the model compounds prepared from bisphenol A with aniline (to form BA-AN BZ) and allylamine (to from BA-AL), as displayed in Figures 7A and 7B, respectively. The char yield for BA-AN BZ was 35.8%, but it was 24.7% for BA-AL BZ. Furthermore, upon comparison of *p*BDDSQ-AN and *o*BDDSQ-AN, the value of T_{d10} and the char yield of *p*BDDSQ-AN were both higher than those of *o*BDDSQ-AN; we also observed this behavior when comparing *p*BDDSQ-AL and *o*BDDSQ-AL. As a result, the *para*-substitution of the aminophenol units in *p*BDDSQ-AN

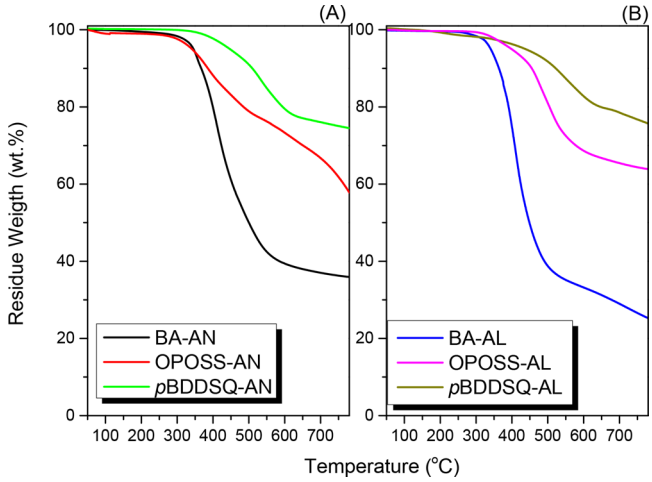

Figure 7. TGA traces of (A) BA-AN, OPOSS-AN, and *p*BDDSQ-AN and (B) BA-AL, OPOSS-AL, and *p*BDDSQ-AL.

and *p*BDDSQ-AL enhanced the thermal stability relative to that of the *ortho*-substitution of the aminophenol units in the *o*BDDSQ-AN and *o*BDDSQ-AL BZ monomers after thermal curing (Scheme 2d). After thermal curing at 270 °C, the thermal stability and char yield followed the order *p*BDDSQ-AN = *p*BDDSQ-AL (T_d, 521 °C; char yield, 75 wt %) > *o*BDDSQ-AN (T_d, 494 °C; char yield, 72.7 wt %) > *o*BDDSQ-AL (T_d, 471 °C; char yield, 67.2 wt %). Nevertheless, although *o*BDDSQ-AL provided the lowest value of T_{d10} (471 °C) and the lowest char yield (67.2%) among these four DDSQ-functionalized BZs after thermal curing, it exhibited significantly greater thermal stability than its model compound, the BA-AL BZ monomer, which had a value of T_{d10} of 360 °C and a char yield of 24.7%, as displayed in Figure 7B. Therefore, the incorporation of the DDSQ inorganic nanoparticles into these typical BZ monomers did indeed enhance the thermal stability significantly. These high char yield of PBZ/DDSQ hybrids could have potential applications in flame retardancy, coating, and advanced composites.[1] We also used SEM and TEM imaging to investigate the homogeneity of the dispersions of the DDSQ nanoparticles in these four DDSQ-functionalized PBZs after thermal curing. We observed a featureless morphology with no discernible phase separation for *p*BDDSQ-AN after thermal curing (Figure 8a,b), indicating that the DDSQ nanoparticles were dispersed well in the PBZ matrix. EDX spectroscopic Si-, N-, and O-mapping of *p*BDDSQ-AN after thermal curing also indicated that the DDSQ nanoparticles were dispersed homogeneously on the surface (Figure 8c–f). The green points in Figure 8c represent the DDSQ-enriched regions—suggesting no aggregation and many uniform spherical nanoparticles. The SEM, TEM, and EDX spectroscopic images of the other three DDSQ-functionalized PBZs are provided in Figures S5 and S7; all of these data are consistent with the DDSQ nanoparticles being dispersed well also within these three PBZ matrices.

Next, we compared the thermal stabilities of our composites with those of octa-BZ-functionalized POSS compounds based on aniline (OPOSS-AN)[47] and allylamine (OPOSS-AL)[48] (Figure 7). The values of T_{d10} and the char yields were 366 °C and 35.8%, respectively, for BA-AN, 385 °C and 55.8%, respectively, for OPOSS-AN, and 521 °C and 75%, respectively, for *p*BDDSQ-AN (Figure 7A); they were 364 °C and 24.7%, respectively, for BA-AL, 455 °C and 63.8%,

DOI: 10.1021/acs.macromol.8b02207
Macromolecules 2018, 51, 9602–9612

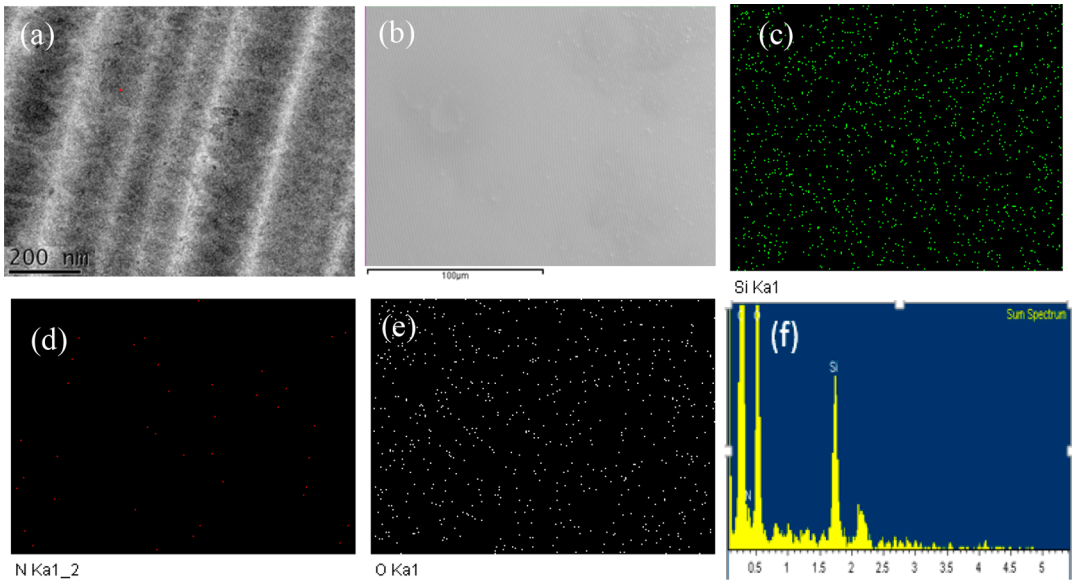

Figure 8. (a) TEM, (b) SEM, (c) Si-mapping, (d) N-mapping, (e) O-mapping, and (f) EDX analyses of the *p*BDDSQ-AN BZ monomer after thermal curing.

respectively, for OPOSS-AL, and 521 °C and 75%, respectively, for *p*BDDSQ-AL (Figure 7B). The incorporation of POSS nanoparticles (di- or octafunctional) into the BZ monomers could indeed enhance the thermal stability significantly, through network formation. In these PBZ/DDSQ hybrids, the DDSQ derivatives could form a ceramic superficial layer during the early stage of combustion due to the relatively lower surface energy of the DDSQ structure, with this inorganic ceramic structure limiting heat transfer and protecting the underlying PBZ while also hampering the diffusion of oxygen. Furthermore, the difunctionalized BZs based on DDSQ (e.g., *p*BDDSQ-AN and *p*BDDSQ-AL) exhibited thermal stability superior to that of the octafunctionalized BZs based on $Q_8M_8^H$ (e.g., OPOSS-AN and OPOSS-AL). The BDDSQ exhibited excellent thermal properties because it was synthesized from the highly aromatic DDSQ, in contrast to the highly methylated $Q_8M_8^H$.[66] In addition, loose structures of OPOSS-AN and OPOSS-AL would form after thermal curing due to the octafunctional topological structure[44,45] derived from $Q_8M_8^H$, and thus, their thermal stabilities were not higher than those of the compounds derived from the DDSQ structure.

Based on our analyses above, the *ortho*-substitution of the aminophenol units in *o*BDDSQ-AN and *o*BDDSQ-AL led to lower thermal stability than did the *para*-substitution of the aminophenol units. Based on our TGA analyses of *o*BDDSQ-AN and *o*BDDSQ-AL in Figures 5C and 5D, respectively, the first decomposition occurred in the range 250−350 °C, caused by the heat polymerization of the BZ unit from the *ortho*-imide PBZ and its partial decomposition prior to transformation into the PBO.[67] The second weight loss in the range 350−450 °C resulted from the release of CO_2 to form the PBO (Scheme 2e). The main degradation was observed in the range 500−650 °C, corresponding to decomposition of the oxazole ring or other units.[58−62] To investigate the thermal stability of the formation of their PBOs, we performed TGA analyses of these four DDSQ-functionalized PBZs after thermal annealing at 450 °C for 2 h (Figure 9). The thermal stabilities of all of the DDSQ-functionalized PBZs were superior after thermal

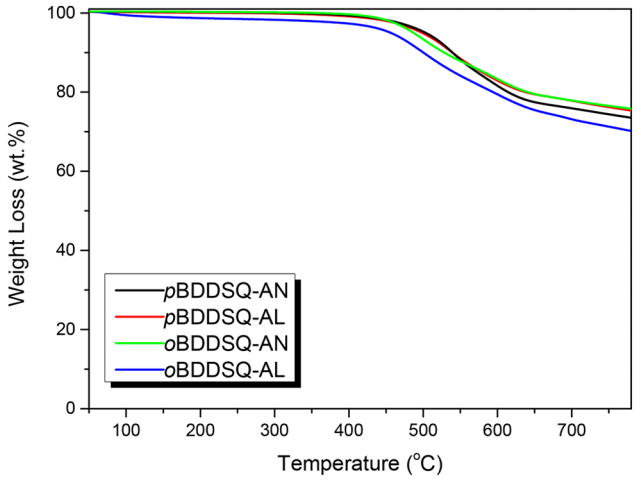

Figure 9. TGA traces of the four DDSQ-functionalized BZ after thermal treatment at 450 °C.

treatment. For example, the values of T_d of *p*BDDSQ-AN and *p*BDDSQ-AN both increased from 521 to 539 °C; for *o*BDDSQ-AN it increased from 494 to 528 °C; and for *o*BDDSQ-AL it increased from 471 to 500 °C. More interestingly, the char yields for the *para*-substituted *p*BDDSQ-AN and *p*BDDSQ-AL remained constant (ca. 75%) after thermal treatment, whereas those of the *ortho*-substituted *o*BDDSQ-AN and *o*BDDSQ-AL increased from 72.7 to 76.0% and from 67.2 to 69.0%, respectively, indicating that the PBO may have formed after thermal treatment to increase the char yield, but the *para*-substituted imide unit might not have formed the PBO. As a result, *o*BDDSQ-AN displayed a char yield even higher than those of the *para*-substituted *p*BDDSQ-AN and *p*BDDSQ-AL. To confirm the formation of PBO after thermal treatment, we used the FTIR spectra after the thermal curing of *o*BDDSQ-AN at 270 °C and thermal treatment at 450 °C as displayed in Figure S8. The asymmetric and symmetric imide C═O stretching were observed at 1714 and 1636 cm^{-1} (Figure S8a); however, a

DOI: 10.1021/acs.macromol.8b02207
Macromolecules 2018, 51, 9602−9612

new absorption appeared at 1596 cm^{-1}, corresponding to the C═N stretching of the benzoxazole. Meanwhile, the imide C═O stretching was significantly decreased after thermal treatment at 450 °C as displayed in Figure S8b, suggesting that the thermal conversion of *o*BDDSQ-AN into the PBO after thermal treatment.[68] The allyl group in *ortho*-imide BZ monomer may not have been useful because it formed an asymmetric cross-linking structure through its further thermal curing; it may also have induced steric hindrance with the *ortho*-imide BZ structure to reduce the thermal stability and char yield.

CONCLUSION

We have synthesized four DDSQ-functionalized BZ monomers, whose structures we confirmed through FTIR, NMR, and MALDI-TOF mass spectral analyses. All of these PBZ/DDSQ hybrids displayed higher thermal stabilities and higher char yields after thermal curing compared with those of traditional typical BZs (e.g., the BA-AN monomer prepared without DDSQ inorganic nanoparticles). The DDSQ inorganic nanoparticles were dispersed well within these PBZ matrices, based on SEM and TEM imaging. More interestingly, the char yield of the *ortho*-substituted *o*BDDSQ-AN increased from 72.7% before thermal treatment to 76.0% after thermal treatment at 450 °C, indicating that the PBO had formed.

ASSOCIATED CONTENT

Supporting Information

The Supporting Information is available free of charge on the ACS Publications website at DOI: 10.1021/acs.macromol.8b02207.

Peak assignment of NMR, FTIR, MALDI-TOF mass spectra, DSC, SEM and TEM images of DDSQ-functionalized benzoxazine monomers (DOCX)

AUTHOR INFORMATION

Corresponding Author

*E-mail: kuosw@faculty.nsysu.edu.tw.

ORCID

Shiao-Wei Kuo: 0000-0002-4306-7171

Notes

The authors declare no competing financial interest.

ACKNOWLEDGMENTS

This study was supported financially by the Ministry of Science and Technology, Taiwan, under Contracts MOST 106-2221-E-110-067-MY3 and 105-2221-E-110-092-MY3. This work is also supported by Center of Crystal Research at National Sun Yat-sen University.

REFERENCES

(1) Ishida, H. In *Handbook of Polybenzoxazine Resins*; Ishida, H., Agag, T., Eds.; Elsevier: Amsterdam, 2011.

(2) Wang, C. F.; Su, Y. C.; Kuo, S. W.; Huang, C. F.; Sheen, Y. C.; Chang, F. C. Low-Surface-Free-Energy Materials Based on Polybenzoxazines. *Angew. Chem., Int. Ed.* **2006**, *45*, 2248−2251.

(3) Froimowicz, P.; Han, L.; Graf, R.; Ishida, H.; Arza, C. R. Design, Synthesis, Characterization, and Polymerization of Fused-Ring Naphthoxazine Resins. *Macromolecules* **2017**, *50*, 9249−9256.

(4) Sawaryn, C.; Landfester, K.; Taden, A. Benzoxazine miniemulsions stabilized with polymerizable nonionic benzoxazine surfactants. *Macromolecules* **2010**, *43*, 8933−8941.

(5) Arslan, M.; Kiskan, B.; Yagci, Y. Benzoxazine-Based Thermosets with Autonomous Self-Healing Ability. *Macromolecules* **2015**, *48*, 1329−1334.

(6) Wang, M. W.; Jeng, R. J.; Lin, C. H. Study on the Ring-Opening Polymerization of Benzoxazine through Multisubstituted Polybenzoxazine Precursors. *Macromolecules* **2015**, *48*, 530−535.

(7) Wang, S.; Li, W. C.; Hao, G. P.; Hao, Y.; Sun, Q.; Zhang, X. Q.; Lu, A. H. Temperature-Programmed Precise Control over the Sizes of Carbon Nanospheres Based on Benzoxazine Chemistry. *J. Am. Chem. Soc.* **2011**, *133*, 15304−15307.

(8) Hao, G. P.; Li, W. C.; Qian, D.; Wang, G. H.; Zhang, W. P.; Zhang, T.; Wang, A. Q.; Schuth, F.; Bongard, H. J.; Lu, A. H. Structurally Designed Synthesis of Mechanically Stable Poly(benzoxazine-co-resol)-Based Porous Carbon Monoliths and Their Application as High-Performance CO_2 Capture Sorbents. *J. Am. Chem. Soc.* **2011**, *133*, 11378−11388.

(9) Zhao, J.; Gilani, M. R. H. S.; Lai, J.; Nsabimana, A.; Liu, Z.; Luque, R.; Xu, G. Autocatalysis Synthesis of Poly(benzoxazine-*co*-resol)-Based Polymer and Carbon Spheres. *Macromolecules* **2018**, *51*, 5494−5500.

(10) Zhang, S.; Ran, Q.; Fu, Q.; Gu, Y. Preparation of Transparent and Flexible Shape Memory Polybenzoxazine Film through Chemical Structure Manipulation and Hydrogen Bonding Control. *Macromolecules* **2018**, *51*, 6561−6570.

(11) Kaya, G.; Kiskan, B.; Yagci, Y. Phenolic Naphthoxazines as Curing Promoters for Benzoxazines. *Macromolecules* **2018**, *51*, 1688−1695.

(12) Wang, Y. X.; Ishida, H. Cationic ring-opening polymerization of benzoxazines. *Polymer* **1999**, *40*, 4563−4570.

(13) Sudo, A.; Kudoh, R.; Nakayama, H.; Arima, K.; Endo, T. Selective Formation of Poly(N,O-acetal) by Polymerization of 1,3-Benzoxazine and Its Main Chain Rearrangement. *Macromolecules* **2008**, *41*, 9030−9034.

(14) Li, X.; Xia, Y.; Xu, W.; Ran, Q.; Gu, Y. The curing procedure for a benzoxazine−cyanate−epoxy system and the properties of the terpolymer. *Polym. Chem.* **2012**, *3*, 1629−1633.

(15) Hu, W. H.; Huang, K. W.; Kuo, S. W. Heteronucleobase-functionalized benzoxazine: synthesis, thermal properties, and self-assembled structure formed through multiple hydrogen bonding interactions. *Polym. Chem.* **2012**, *3*, 1546−1554.

(16) Lin, R. C.; Kuo, S. W. Benzoxazine/Triphenylamine-Based Dendrimers Prepared through Facile One-Pot Mannich Condensations. *Macromol. Rapid Commun.* **2017**, *38*, 1700251.

(17) Wu, J. Y.; Mohamed, M. G.; Kuo, S. W. Directly synthesized nitrogen-doped microporous carbons from polybenzoxazine resins for carbon dioxide capture. *Polym. Chem.* **2017**, *8*, 5481−5489.

(18) Low, H. Y.; Ishida, H. Mechanistic study on the thermal decomposition of polybenzoxazines: Effects of aliphatic amines. *J. Polym. Sci., Part B: Polym. Phys.* **1998**, *36*, 1935.

(19) Agag, T.; Takeichi, T. Synthesis and Characterization of Novel Benzoxazine Monomers Containing Allyl Groups and Their High Performance Thermosets. *Macromolecules* **2003**, *36*, 6010−6017.

(20) Agag, T.; Takeichi, T. Novel Benzoxazine Monomers Containing *p*-Phenyl Propargyl Ether: Polymerization of Monomers and Properties of Polybenzoxazines. *Macromolecules* **2001**, *34*, 7257−7263.

(21) Chen, C. H.; Lin, C. H.; Wong, T. I.; Wang, M. W.; Juang, T. Y. Thermosets derived from diallyl-containing main-chain type benzoxazine polymers. *Polymer* **2018**, *149*, 286−293.

(22) Zou, X.; Yang, X.; Xu, M.; Jia, K.; Liu, X. Curing behaviors and properties of allyl- and benzoxazine-functional phthalonitrile with improved processability. *J. Polym. Res.* **2016**, *23*, 2.

(23) Huang, J. M.; Kuo, S. W.; Lee, Y. J.; Chang, F. C. Synthesis and Characterization of a Vinyl-Terminated Benzoxazine Monomer and its Blends with Poly(ethylene oxide). *J. Polym. Sci., Part B: Polym. Phys.* **2007**, *45*, 644−653.

(24) Demir, K. D.; Kiskan, B.; Yagci, Y. Thermally Curable Acetylene-Containing Main-Chain Benzoxazine Polymers via Sonogashira Coupling Reaction. *Macromolecules* **2011**, *44*, 1801−1807.

DOI: 10.1021/acs.macromol.8b02207
Macromolecules 2018, 51, 9602−9612

(25) Zhang, K.; Yu, X. Catalyst-Free and Low-Temperature Terpolymerization in a Single-Component Benzoxazine Resin Containing Both Norbornene and Acetylene Functionalities. *Macromolecules* **2018**, *51*, 6524−6533.
(26) Lin, C. H.; Huang, S. J.; Wang, P. J.; Lin, H. T.; Dai, S. A. Miscibility, Microstructure, and Thermal and Dielectric Properties of Reactive Blends of Dicyanate Ester and Diamine-Based Benzoxazine. *Macromolecules* **2012**, *45*, 7461−7466.
(27) Su, Y. C.; Kuo, S. W.; Yei, D. R.; Xu, H.; Chang, F. C. Thermal Property and Hydrogen Bonding in Polymer Blend of Polybenzoxazine/ Poly(N-vinyl-2-pyrrolidone). *Polymer* **2003**, *44*, 2187−2191.
(28) Brown, E. A.; Rider, D. A. Pegylated Polybenzoxazine Networks with Increased Thermal Stability from Miscible Blends of Tosylated Poly(ethylene glycol) and a Benzoxazine Monomer. *Macromolecules* **2017**, *50*, 6468−6481.
(29) Selvi, M.; Devaraju, S.; Sethuraman, K.; Alagar, M. Carbon black−polybenzoxazine nanocomposites for high *K* dielectric applications. *Polym. Compos.* **2014**, *35*, 2121−2128.
(30) Chen, Q.; Xu, R.; Yu, D. Multiwalled carbon nanotube/polybenzoxazine nanocomposites: Preparation, characterization and properties. *Polymer* **2006**, *47*, 7711−7719.
(31) Wang, Y. H.; Chang, C. M.; Liu, Y. L. Benzoxazine-functionalized multi-walled carbon nanotubes for preparation of electrically-conductive polybenzoxazines. *Polymer* **2012**, *53*, 106−112.
(32) Yang, C. C.; Lin, Y. C.; Wang, P. I.; Liaw, D. J.; Kuo, S. W. Polybenzoxazine/single-walled carbon nanotube nanocomposites stabilized through noncovalent bonding interactions. *Polymer* **2014**, *55*, 2044−2050.
(33) Mohamed, M. G.; Hsu, K. C.; Kuo, S. W. Bifunctional polybenzoxazine nanocomposites containing photo-crosslinkable coumarin units and pyrene units capable of dispersing single-walled carbon nanotubes. *Polym. Chem.* **2015**, *6*, 2423−2433.
(34) Mohamed, G. M.; Hsiao, C. H.; Luo, F.; Dai, L.; Kuo, S. W. Multifunctional polybenzoxazine nanocomposites containing photo-responsive azobenzene units, catalytic carboxylic acid groups, and pyrene units capable of dispersing carbon nanotubes. *RSC Adv.* **2015**, *5*, 45201−45212.
(35) Shih, H. K.; Hsieh, C. C.; Mohamed, M. G.; Zhu, C. Y.; Kuo, S. W. Ternary polybenzoxazine/POSS/SWCNT hybrid nanocomposites stabilized through supramolecular interactions. *Soft Matter* **2016**, *12*, 1847−1856.
(36) Arza, C. R.; Ishida, H.; Maurer, F. H. Quantifying Dispersion in Graphene Oxide/Reactive Benzoxazine Monomer Nanocomposites. *Macromolecules* **2014**, *47*, 3685−3692.
(37) Zeng, M.; Wang, J.; Li, R.; Liu, J.; Chen, W.; Xu, Q.; Gu, Y. The curing behavior and thermal property of graphene oxide/benzoxazine nanocomposites. *Polymer* **2013**, *54*, 3107−3116.
(38) Meng, F.; Ishida, H.; Liu, X. Introduction of benzoxazine onto the graphene oxide surface by click chemistry and the properties of graphene oxide reinforced polybenzoxazine nanohybrids. *RSC Adv.* **2014**, *4*, 9471−9475.
(39) Kumar, R. S.; Padmanathan, N.; Alagar, M. Design of hydrophobic polydimethylsiloxane and polybenzoxazine hybrids for interlayer low *k* dielectrics. *New J. Chem.* **2015**, *39*, 3995−4008.
(40) Chen, K. C.; Li, H. T.; Huang, S. C.; Chen, W. C.; Sun, K. W.; Chang, F. C. Synthesis and performance enhancement of novel polybenzoxazines with low surface free energy. *Polym. Int.* **2011**, *60*, 1089−1096.
(41) Fu, H. K.; Huang, C. F.; Kuo, S. W.; Lin, H. C.; Yei, D. R.; Chang, F. C. Effect of an Organically Modified Nanoclay on Low-Surface-Energy Materials of Polybenzoxazine. *Macromol. Rapid Commun.* **2008**, *29*, 1216−1220.
(42) Cui, H. W.; Kuo, S. W. Nanocomposites of polybenzoxazine and exfoliated montmorillonite using a polyhedral oligomeric silsesquioxane surfactant and click chemistry. *J. Polym. Res.* **2013**, *20*, 114.
(43) Lee, Y. J.; Kuo, S. W.; Su, Y. C.; Chen, J. K.; Tu, C. W.; Chang, F. C. Syntheses, Thermal properties, and Phase Morphologies of Novel Benzoxazines Functionalized with Polyhedral Oligomeric Silsesquioxane (POSS) Nanocomposites. *Polymer* **2004**, *45*, 6321−6331.
(44) Lee, Y. J.; Huang, J. M.; Kuo, S. W.; Chen, J. K.; Chang, F. C. Synthesis and Characterizations of a Vinyl-terminated Benzoxazine Monomer and its Blending with Polyhedral Oligomeric Silsesquioxane (POSS). *Polymer* **2005**, *46*, 2320−2330.
(45) Lee, Y. J.; Kuo, S. W.; Huang, C. F.; Chang, F. C. Synthesis and Characterization of Polybenzoxazine Networks Nanocomposites Containing Multifunctional Polyhedral Oligomeric Silsesquioxane (POSS). *Polymer* **2006**, *47*, 4378−4386.
(46) Huang, J. M.; Kuo, S. W.; Huang, H. J.; Wang, Y. X.; Chen, Y. T. Preparation of VB-a/POSS Hybrid Monomer and its Polymerization of Polybenzoxazine/POSS Hybrid Nanocomposites. *J. Appl. Polym. Sci.* **2009**, *111*, 628−634.
(47) Wu, Y. C.; Kuo, S. W. Synthesis and Characterization of Polyhedral Oligomeric Silsesquioxane (POSS) with Multifunctional Benzoxazine Groups through Click Chemistry. *Polymer* **2010**, *51*, 3948−3955.
(48) Huang, K. W.; Kuo, S. W. High Performance Polybenzoxazine Nanocomposites Containing Multifunctional POSS Cores Presenting Vinyl-Terminated Benzoxazine Groups. *Macromol. Chem. Phys.* **2010**, *211*, 2301−2311.
(49) Kuo, S. W.; Chang, F. C. POSS related Polymer Nanocomposites. *Prog. Polym. Sci.* **2011**, *36*, 1649−1696.
(50) Hu, W. H.; Huang, K. W.; Chiou, C. W.; Kuo, S. W. Complementary Multiple Hydrogen Bonding Interactions Induce the Self-Assembly of Supramolecular Structures from Heteronucleobase-Functionalized Benzoxazine and Polyhedral Oligomeric Silsesquioxane Nanoparticles. *Macromolecules* **2012**, *45*, 9020−9028.
(51) Mohamed, M. G.; Kuo, S. W. Polybenzoxazine/Polyhedral Oligomeric Silsesquioxane (POSS) Nanocomposites. *Polymers* **2016**, *8*, 225.
(52) Chen, Q.; Xu, R.; Zhang, J.; Yu, D. Polyhedral Oligomeric Silsesquioxane (POSS) Nanoscale Reinforcement of Thermosetting Resin from Benzoxazine and Bisoxazoline. *Macromol. Rapid Commun.* **2005**, *26*, 1878−1882.
(53) Tseng, M. C.; Liu, Y. L. Preparation, morphology, and ultra-low dielectric constants of benzoxazine-based polymers/polyhedral oligomeric silsesquioxane (POSS) nanocomposites. *Polymer* **2010**, *51*, 5567−5575.
(54) Zhang, K.; Zhuang, Q.; Liu, X.; Yang, G.; Cai, R.; Han, Z. A New Benzoxazine Containing Benzoxazole-Functionalized Polyhedral Oligomeric Silsesquioxane and the Corresponding Polybenzoxazine Nanocomposites. *Macromolecules* **2013**, *46*, 2696−2704.
(55) Liao, Y. T.; Lin, Y. C.; Kuo, S. W. Highly Thermally Stable, Transparent, and Flexible Polybenzoxazine Nanocomposites by Combination of Double-Decker-Shaped Polyhedral Silsesquioxanes and Polydimethylsiloxane. *Macromolecules* **2017**, *50*, 5739−5747.
(56) Liu, N.; Li, L.; Wang, L.; Zheng, S. Organic-inorganic polybenzoxazine copolymers with double decker silsesquioxanes in the main chains: Synthesis and thermally activated ring-opening polymerization behavior. *Polymer* **2017**, *109*, 254−265.
(57) Zhang, C.; Liu, N.; Li, L.; Wang, L.; Zheng, S. Polybenzoxazine nanocomposites containing 3,13-Diglycidyl double-decker silsesquioxane. *Polym. Compos.* **2017**, *38*, 827−836.
(58) Zhang, K.; Ishida, H. An anomalous trade-off effect on the properties of smart*ortho*-functional benzoxazines. *Polym. Chem.* **2015**, *6*, 2541−2550.
(59) Zhang, K.; Ishida, H. Smart synthesis of high-performance thermosets based on *ortho*-amide−imide functional benzoxazines. *Front. Mater.* **2015**, DOI: 10.3389/fmats.2015.00005.
(60) Zhang, K.; Ishida, H. Thermally stable polybenzoxazines via *ortho*-norbornene functional benzoxazine monomers: Unique advantages in monomer synthesis, processing and polymer properties. *Polymer* **2015**, *66*, 240−248.
(61) Zhang, K.; Liu, J.; Ishida, H. An Ultrahigh Performance Cross-Linked Polybenzoxazole via Thermal Conversion from Poly(benzoxazine amic acid) Based on Smart *o*-Benzoxazine Chemistry. *Macromolecules* **2014**, *47*, 8674−8681.

DOI: 10.1021/acs.macromol.8b02207
Macromolecules 2018, 51, 9602−9612

(62) Zhang, K.; Han, L.; Froimowicz, P.; Ishida, H. A Smart Latent Catalyst Containing *o*-Trifluoroacetamide Functional Benzoxazine: Precursor for Low Temperature Formation of Very High Performance Polybenzoxazole with Low Dielectric Constant and High Thermal Stability. *Macromolecules* **2017**, *50*, 6552−6560.
(63) Wu, S.; Hayakawa, T.; Kikuchi, R.; Grunzinger, S. J.; Kakimoto, M.; Oikawa, H. Synthesis and characterization of semiaromatic polyimides containing POSS in main chain derived from double-decker-shaped silsesquioxane. *Macromolecules* **2007**, *40*, 5698−5705.
(64) Wu, S.; Hayakawa, T.; Kakimoto, M.; Oikawa, H. Synthesis and Characterization of Organosoluble Aromatic Polyimides Containing POSS in Main Chain Derived from Double-Decker-Shaped Silsesquioxane. *Macromolecules* **2008**, *41*, 3481−3487.
(65) Zhang, L.; Zhu, Y. J.; Li, D.; Wang, M.; Chen, H. B.; Wu, J. S. Preparation and characterization of fully renewable polybenzoxazines from monomers containing multi-oxazine rings. *RSC Adv.* **2015**, *5*, 96879−96887.
(66) Yu, C. Y.; Kuo, S. W. Phenolic Functionality of Polyhedral Oligomeric Silsesquioxane Nanoparticles Affects Self-Assembly Supramolecular Structures of Block Copolymer Hybrid Complexes. *Ind. Eng. Chem. Res.* **2018**, *57*, 2546−2559.
(67) El-Mahdy, A. F. M.; Kuo, S. W. Direct synthesis of poly (benzoxazine imide) from an ortho-benzoxazine: its thermal conversion to highly cross-linked polybenzoxazole and blending with poly (4-vinylphenol). *Polym. Chem.* **2018**, *9*, 1815−1826.
(68) Calle, M.; Lozano, A. E.; Lee, Y. M. Formation of thermally rearranged (TR) polybenzoxazoles: Effect of synthesis routes and polymer form. *Eur. Polym. J.* **2012**, *48*, 1313−1322.

DOI: 10.1021/acs.macromol.8b02207
Macromolecules 2018, 51, 9602−9612